Chemistry–A European Journal

Research Article
doi.org/10.1002/chem.202500607

Chemistry Europe
European Chemical Societies Publishing

www.chemeurj.org

Relaxing amid Three: Slow Magnetization Relaxation in Three-Coordinate Chromium(II) N-Heterocyclic Carbene Complexes

Gabriela Handzlik,[a] Irene Ligielli,[b] Sakshi Nain,[c] Rishu Khurana,[c] Md. Ehesan Ali,*[c] Evangelos Papangelis,[b] Charalampos Papapanagis,[b] Corinne Bailly,[d] Nikolaos Tsoureas,[b] Marianna Danopoulou,[b] Costas Bethanis,[e] Pierre Braunstein,*[f] Dawid Pinkowicz,*[a] Jurek Krzystek,*[g] Panayotis Kyritsis,*[b] and Andreas A. Danopoulos*[b]

Dedicated to Professor Christina-Anna Mitsopoulou on the occasion of her retirement

Three-coordinate, paramagnetic Cr^{II} complexes of type $[Cr(amido)_nBn_m(NHC)]$, NHC = N, N′-bis-(2,4,6-trimethylphenyl)-imidazol-2-ylidene (IMes); N, N′-bis-(2,6-di-*iso*propylphenyl)-imidazol(in)-2-ylidene, (S)IDiPP; N, N′-bis-(2,6-di-*iso*propylphenyl)-imidazol-4-ylidene, (*a*IDiPP); amido = $N(SiMe_3)_2$, NH(DiPP); Bn = benzyl, n = 2, m = 0; n = 1, m = 1, were prepared by substitution or aminolysis and thermolysis methods from $[Cr\{N(SiMe_3)_2\}_2(THF)_2]$ or $[CrBn_2((S)IDiPP)]$, respectively. Depending on the nature of the NHC and the amido ligands, different geometries at Cr^{II} (ranging from distorted trigonal planar, to extended Y-, compressed Y-, and distorted T-shaped) and conformations, were observed. HFEPR spectroscopy was employed to accurately determine spin Hamiltonian parameters, consisting of zero-field splitting (axial *D* and rhombic *E* components) and g-values, of five *S* = 2 complexes exhibiting *D* and *E/D* in the range from −2.98 to −1.63 cm^{-1} and 0.026 − 0.069, respectively. AC magnetometry established slow magnetization relaxation in three complexes, operating by Raman or combined Raman-Orbach processes. *Ab initio* calculations provided computed zfs values, in good agreement with those obtained by HFEPR. Magnetostructural comparisons are made within this three-coordinate Cr^{II} family, as well as with previously studied two- or four- coordinate Cr^{II} complexes.

1. Introduction

Following extensive studies on polynuclear complexes that exhibit slow magnetization relaxation (i.e., single molecule magnets, SMMs),[1] research effort has shifted to mono-[2–5] and, more recently, bi-nuclear[6] *f*-block element SMMs,[7] leading to "tailor-made" lanthanide complexes with high effective barrier of magnetization reversal (U_{eff}), and blocking temperatures (T_B) approaching[3,5] or surpassing[4,6] 77 K. Moreover, detailed mapping of the dynamic magnetic behavior of mononuclear 3*d*-metal complexes has been under intense scrutiny,[8–10] aiming at validating magnetostructural correlations related to slow magnetization relaxation. Accordingly, numerous $3d^n$-metal complexes (n = 5 − 9) have emerged as mononuclear SMMs, either in the presence ("field-induced") or, less frequently, in the absence of a direct-current (DC)

[a] G. Handzlik, D. Pinkowicz
Faculty of Chemistry, Jagiellonian University, Gronostajowa 2, Krakow 30–387, Poland
E-mail: dawid.pinkowicz@uj.edu.pl

[b] I. Ligielli, E. Papangelis, C. Papapanagis, N. Tsoureas, M. Danopoulou, P. Kyritsis, A. A. Danopoulos
Laboratory of Inorganic Chemistry, National and Kapodistrian University of Athens, Panepistimiopolis Zografou, Athens 15771, Greece
E-mail: kyritsis@chem.uoa.gr
adanop@chem.uoa.gr

[c] S. Nain, R. Khurana, M. E. Ali
Institute of Nano Science and Technology, Sector-81, Mohali, Punjab 140306, India
E-mail: ehesan.ali@inst.ac.in

[d] C. Bailly
Service de Radiocristallographie, Fédération de Chimie, 1 rue Blaise Pascal, BP 296/R8, Strasbourg Cedex 67008, France

[e] C. Bethanis
Physics Laboratory, Department of Biotechnology, Agricultural University of Athens, 75 Iera Odos, Athens 11855, Greece

[f] P. Braunstein
Institut de Chimie UMR 7177, Université de Strasbourg, CNRS, Strasbourg Cedex 67081, France
E-mail: braunstein@unistra.fr

[g] J. Krzystek
National High Magnetic Field Laboratory, Florida State University, Tallahassee, Florida 32310, USA
E-mail: krzystek@magnet.fsu.edu

Supporting information for this article is available on the WWW under https://doi.org/10.1002/chem.202500607

magnetic field.[9,11] The favorable effects of low coordination numbers linked to large U_{eff} due to significant magnetic anisotropy — expressed by the axial (D) and rhombic (E) components of the zero-field splitting (ZFS) — have been demonstrated for linear Fe^{I} alkyls[12] and amides,[13] linear and bent Fe^{II} amides,[14] aryls[15] and linear aryloxides.[16] Moreover, the building of linear coordination spheres by taking advantage of the sterics of the N-heterocyclic carbenes (NHCs) led to the slowly relaxing linear complexes $[Co^{I}(IMes)_2]^{+}$, IMes = 1,3-bis(mesityl)imidazol-2-ylidene;[17] $[Co^{II}(=NAr^{*})(sIDiPP)]$, Ar* = 2,6-dimesitylphenyl, sIDiPP = 1,3-bis(2,6-$iPr_2C_6H_3$)imidazolin-2-ylidene;[18] $[Fe^{I}\{N(SiMe_3)_2\}(IDiPP)]$[13] and $[Ni^{I}(6\text{-IMes})_2]^{+}$, 6-IMes = 1,3-bis(mesityl)-3,4,5,6-tetrahydropyrimidin-2-ylidene;[19] the Co imido species features a remarkable U_{eff} value (413 cm^{-1}).[11] Many three-coordinate complexes of Co^{II},[20–25] Fe^{II},[26,27] and — to a lesser degree — Fe^{III} [28,29] are field-induced mononuclear SMMs, also referred to as single-ion magnets (SIMs).

By contrast, among the $3d^{n}$-metal-complexes (n < 5), only a handful of non-Kramers, $S = 2$, Cr^{II} molecular systems have been identified as field-induced SIMs (Figure 1 and I-IV).[30–34] They feature coordination numbers of four or two in distorted square-planar (CrN_4[31,32] or CrN_2O_2[31]), seesaw (CrN_4[33]) or *quasi*-linear (CrS_2[34]) geometries; the static magnetic properties of twocoordinate bent,[35,36] *quasi*-two-coordinate and T-shaped Cr^{II},[37–39] and square planar[40] Cr^{II} bis(trimethylsilyl)amido complexes have been reported, in conjunction with synthetic studies (Figure 1 and V). Moreover, ab initio computational studies have anticipated "record high" magnetic anisotropy for $[M\{N(SiMe_3)_2\}_3]^{m}$, M = Mn, m = 0; M = Cr, m = −1 (Figure 1 and VI).[41,42] The binuclear $[Cr^{II}\{N(SiiPr_3)_2\}(\mu\text{-Cl})(THF)]_2$ was recently shown to exhibit slow magnetization relaxation even in the absence of a DC field.[43]

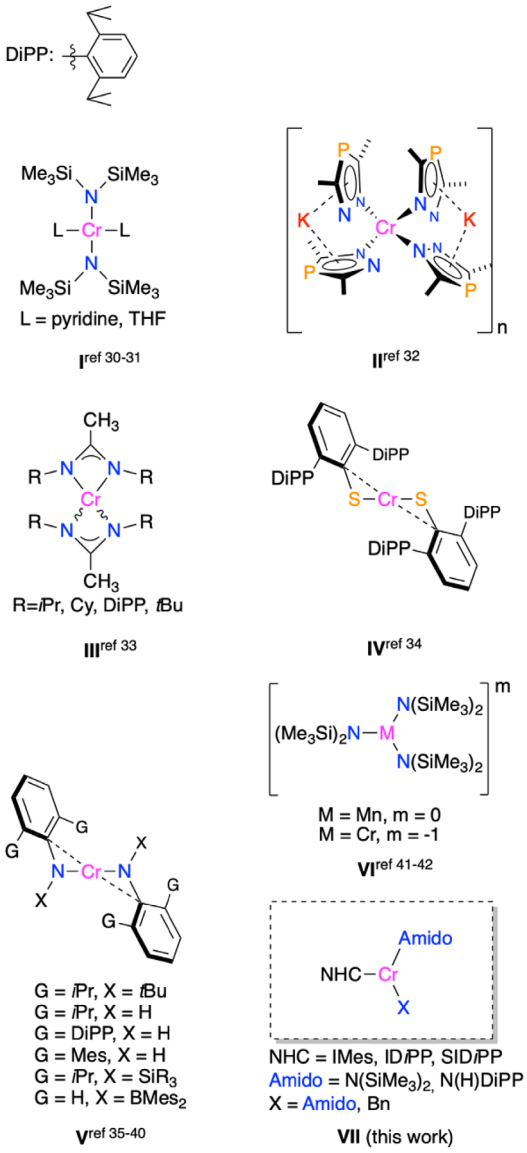

Figure 1. Four-coordinate (I-III) and quasi-linear (IV-V) Cr^{II} complexes exhibiting slow magnetization relaxation; the three-coordinate complexes VI have been predicted, by computation methods, to behave similarly.

2. Results and Discussion

2.1. Synthesis and Structures of the Complexes

In view of the SIM potential of mononuclear three-coordinate 3*d* metal complexes of the type $[M\{N(SiMe_3)_2\}_2]L]$,[44,45] M = Fe, Co; L = IDiPP, sIDiPP *etc.*, we targeted $3d^{4}$ high-spin Cr^{II} bis(trimethylsilylamido) complexes of analogous structure; the electronic and steric opportunities that are offered by the diverse NHC functionalities were also an attractive feature. All three-coordinate complexes of the general type $[Cr(amido)_nBn_m(NHC)]$, where amido = $N(SiMe_3)_2$, NH(DiPP), Bn = benzyl and m+n = 2 that are included in this work, as well as the methodologies employed for their study, are summarized in Table 1.

$[Cr\{N(SiMe_3)_2\}_2(THF)_2]$[31] (**1**) seemed to be a plausible entry to access $[Cr\{N(SiMe_3)_2\}_2\}(NHC)]$ species by "extrusion" of the two THF molecules and introduction of the NHC ligands. In general, the reactions of **1** with the free NHCs proved to be "capricious": the most straightforward reaction of **1** with one equivalent of *freshly prepared* IMes in toluene, proceeded to completion within 5–6 h at 40–50 °C affording after work-up the light-green, extremely air-sensitive, crystalline three-coordinate **3** (Scheme 1).

No other products could be isolated from the reaction medium under these conditions. In contrast, by heating the above reaction mixture at 70 °C for 12 h resulted in gradual darkening of the color, eventually turning dark brown. Work-up as before at this stage gave as product a mixture of co-crystallizing **3** and its cyclometalated complex **3a** (Scheme 4); heating the reaction mixture at higher temperatures resulted in the formation of intractable mixtures. Interestingly, attempts to prepare the SIMes analogue of **3**, SIMes = N, N′-bis-(2,4,6-trimethylphenyl)-imidazolin-2-ylidene, following the same protocol led to the recovery of both unreacted starting materials. Moreover, the "extrusion" of the two THF ligands in **1** by the reaction with one equivalent of IDiPP (as detailed in the ESI), was found to be preferentially carried out in *n*-heptane giving rise to the light green **4**. Complexes analogous to **3** and **4** but bearing as NHCs ^{Me2}CAAC, ^{Et2}CAAC or RE-6 NHC, CAAC = Cyclic Alkyl Amino

Table 1. Summary of three-coordinate complexes of Cr^{II} reported herein and the methodologies employed for their study.

Complex	Empirical name	sc-XRD	μ_{eff} (Evans)	DC magnetometry	AC magnetometry	HFEPR	Computational studies
2b	[Cr(Bn)$_2$(IDiPP)]	Fig. S12	3.87(2)				
2c	[Cr(Bn)$_2$(IDiPP*)]	Fig. 2					
3	[Cr{N(SiMe$_3$)$_2$}$_2$(IMes)]	Fig. 3	4.26(3)	✔	✔	✔	✔
4	[Cr{N(SiMe$_3$)$_2$}$_2$(IDiPP)]	Fig. S15	4.23(2)			✔	✔
5	[Cr(Bn){N(SiMe$_3$)$_2$}(IDiPP)]	Fig. 4	4.02(2)	✔	✔	✔	✔
5b	[Cr(Bn){N(SiMe$_3$)$_2$}(SIDiPP)]	Fig. S17	4.40(2)	✔	✔	✔	✔
6a	[Cr(Bn)(NHDiPP)(IDiPP)]	Fig. 5	4.20(3)				
6b	[Cr(Bn)(NHDiPP)(SIDiPP)]	Fig. S19	3.95(1)	✔	✔		✔
7	[Cr(NHDiPP)$_2$(IDiPP)]	Fig. 6	3.94(1)				
8	[Cr{N(SiMe$_3$)$_2$}$_2$(a-IDiPP)]	Fig. 7	4.14(1)	✔	✔	✔	✔

Abbreviations used throughout the paper: IMes = 1,3-bis(2,4,6-trimethylphenyl)imidazol-2-ylidene; IDiPP = 1,3-bis(2,6-*i*Pr$_2$C$_6$H$_3$)imidazol-2-ylidene; SIDiPP = 1,3-bis(2,6-*i*Pr$_2$C$_6$H$_3$)imidazolin-2-ylidene; *a*-IDiPP = N, N′-bis-(2,6-di-*iso*propylphenyl)-imidazol-4-ylidene; IDiPP* = 1,3-bis(2,6-(Ph$_2$CH)$_2$)-4-(CH$_3$)-C$_6$H$_2$)imidazol-2-ylidene; DiPP = 2,6-di*iso*propyl-phenyl; Bn = benzyl

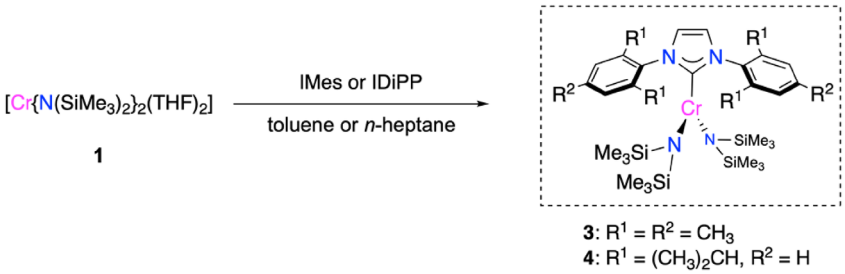

Scheme 1. The synthesis of the three-coordinate Cr^{II} NHC complexes **3** and **4** by THF displacement.

Carbene, RE-6 NHC = 1,3-bis-(2,4,6-trimethylphenyl)-pyrimidin-2-ylidene, following the THF "extrusion" strategy in **1**, could not be obtained, leading instead to the isolation of unreacted starting materials.

In order to access additional ID*i*PP analogues of **4**, the aminolysis of benzyl (Bn) groups in **2a**, **2b,** and **2c** complexes was considered. The known **2a**[46] is available in synthetically useful quantities (routinely at *ca*. 800 mg, as described in the ESI). Moreover, the analogues of **2b** and **2c** obtained as shown in Scheme 2, were targeted in order to control the aminolysis, the subsequent thermal reactivity (viz. normal to abnormal NHC isomerization etc. vide infra) and in order to manipulate the sterics at the primary and secondary coordination spheres of Cr^{II}. Interestingly, although **2b** showed analogous structural characteristics to those of **2a**, complex **2c** revealed counter-intuitive (based on sheer steric arguments) geometrical features and disposition of the Cr and Bn ligands, respectively (vide infra). Despite its interesting structure, the limited availability of **2c** in quantities suitable to carry out further transformations, hampered efforts to study derivatives with the amido ligand scaffolds that are the subject of this work.

Reactions of **2a** and **2b** in neat NH(SiMe$_3$)$_2$ at 50 °C afforded the complexes **5a** and **5b**, respectively, featuring one bis(trimethylsilyl)-amide and one Bn groups attached to the Cr^{II} center. Longer reaction times did not lead to the conversion to the disubstituted bis(trimethylsilyl)-amido species (Scheme 3).

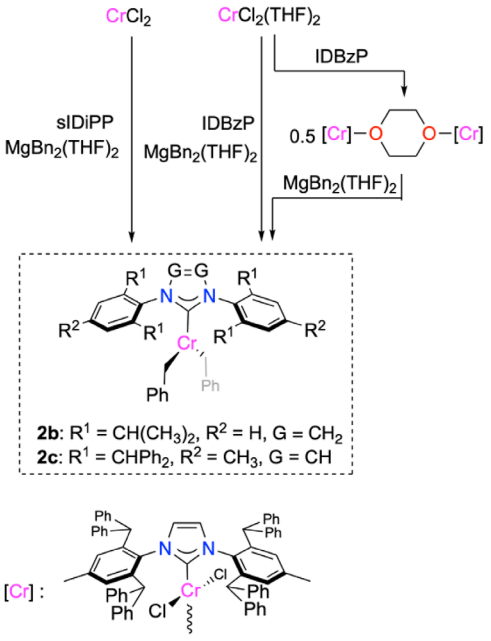

Scheme 2. The synthesis of the dibenzyl analogues **2b** and **2c**.

However, prolonged heating of a solution of **5a** in neat NH(SiMe$_3$)$_2$ at 105 °C produced good yields of complex **8** after crystallization from *n*-hexane or *n*-heptane (Scheme 4). Complex

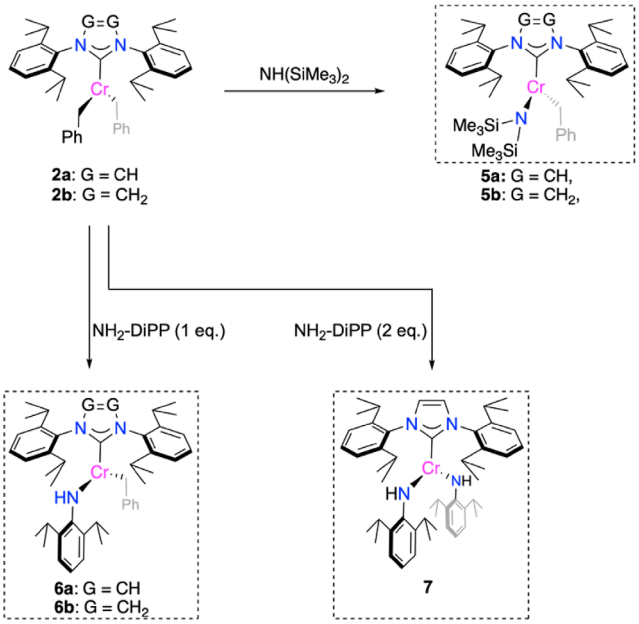

Scheme 3. Aminolysis reactions of **2a** and **2b**.

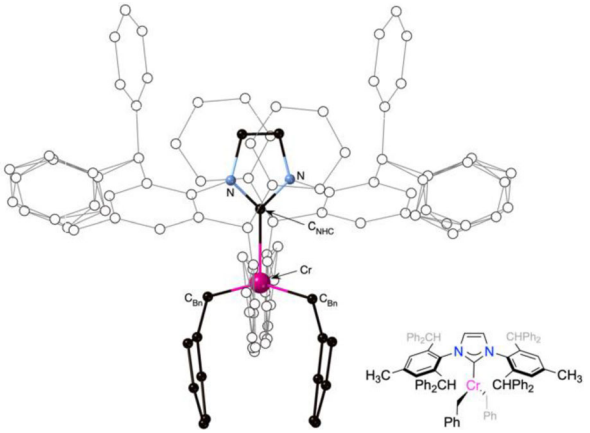

Figure 2. The molecular structure of **2c** with selected metrical data (Å and °) (only one of the two disordered positions of the Bn group are depicted and used for the metrical measurements); one disordered molecule of solvent (ether) is omitted: Cr–C_{NHC} = 2.135(11); Cr–C_{Bn} = 1.85(3); C_{Bn}–Cr–C_{Bn} = 147.2(17); C_{NHC}–Cr–C_{Bn} = 106.4(8); Σ at Cr = 360.0°.

8 features two anionic bis(trimethylsilyl)-amido and one neutral "abnormal", mesoionic NHC (*a*IDi*PP* donors (*a*IDi*PP* = 1,3-bis(2,6-*i*Pr$_2$C$_6$H$_3$)imidazol-4-ylidene), the NHC rearrangement presumably being driven by the release of steric congestion around the metal center. Quantitative yields of **8** could also be obtained directly from **2a** by heating in neat HN(SiMe$_3$)$_2$ at 105 °C for 12 h. Heating of **2b** under the same conditions led to intractable mixtures. Selective, stepwise aminolysis reactions were also carried out by reacting **2a** with one or two equivalents of 2,6-diisopropylaniline which afforded **6a** and **6b**, respectively, featuring one or two anilide ligands at the coordination sphere of the metal center. However, analogous reaction with **2b** gave cleanly only the mono-substituted product **7** (Scheme 3).

Complexes **2b**–**8** are $S = 2$ paramagnets in benzene or toluene solutions (Table S5); the μ_{eff} values obtained are lower than the spin-only value of 4.90 μ_B expected for $3d^4$ complexes, suggesting unquenched orbital angular momentum that contributes to the overall moment, and is lower due to the positive spin – orbit coupling constant. Complexes **2b**–**8** display paramagnetically shifted ^{1}H-NMR spectra that were tentatively assigned, where possible, based on comparison of relevant complexes within the group or previously reported compounds and on integration (Figures S1–S11 in ESI).

The structures of **2b**, **2c**, **3**, **4**, **5a**, **5b**, **6a**, **6b**, **7** and **8** were determined crystallographically; structural molecular models of the complexes **2c**, **3**, **5a**, **6a**, **7** and **8** are shown in Figures 2, 3, 4, 5, 6 and 7, respectively; additional crystallographic data and details are shown in the ESI (Table S1 and Figures S12–S27).

The structure of **2b** (Figure S12) has close similarities with the previously reported structure of **2a**:[46] the Cr center is marginally pyramidalized (Σ = 357.8°) and the coordination angles between the two Bn ligands point to a trigonal geometry distorted towards compressed-Y. The Cr–C_{NHC} distances in both complexes are the same within the measured esds, (2.1146(13) and 2.124(3) Å, respectively); also, in **2b** (as previously seen in **2a**) the Cr–C_{NHC} are significantly shorter than the two Cr–C_{Bn} distances (2.1756(16) and 2.1525(15) Å). As in **2a**, striking departures from the ideal tetrahedral value (109°) of the angles subtended at C_{Bn} are reproduced in **2b**; this phenomenon has been attributed to the

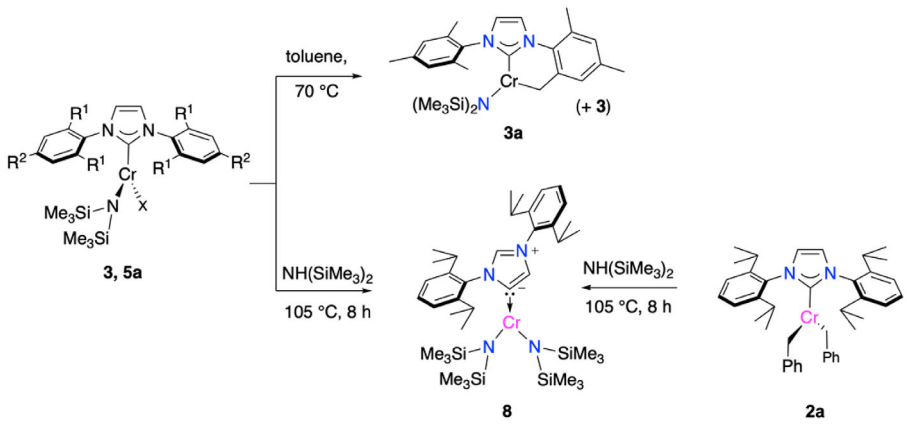

Scheme 4. Thermolysis of the complexes **3**, **5a** and **2a**.

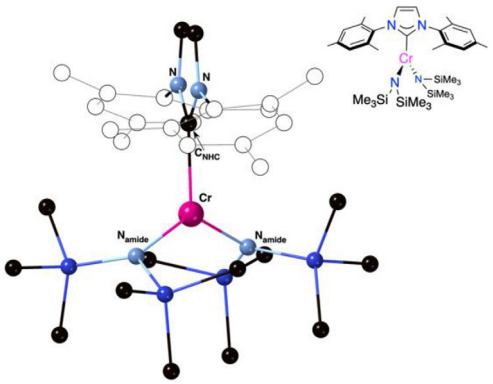

Figure 3. The structure of **3** with selected metrical data (Å and °): Cr–C_{NHC} = 2.156(5); Cr–N_{amide} = 2.016(4) and 2.022(4); C_{NHC}–Cr–N_{amide} = 115.81(17) and 116.73(17); N_{amide}–Cr–N_{amide} = 127.46(17); Σ at Cr = 360.1°.

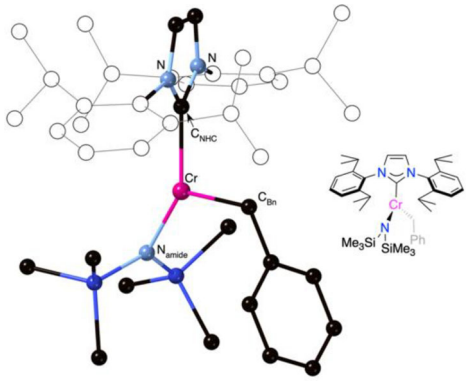

Figure 4. The structure of **5a** with selected metrical data (Å and °): Cr–C_{NHC} = 2.144(2); Cr–N_{amide} = 1.9748(19) Cr–C_{Bn} 2.092(2); $C_{NH\ C}$–Cr–C_{Bn} = 93.33(9); C_{NHC}–Cr–N_{amide} = 148.86(8); C_{Bn}–Cr–N_{amide} = 117.74(9); Cr–C_{Bn}–C_{ipso} = 115.65(16); Σ at Cr = 359.8.

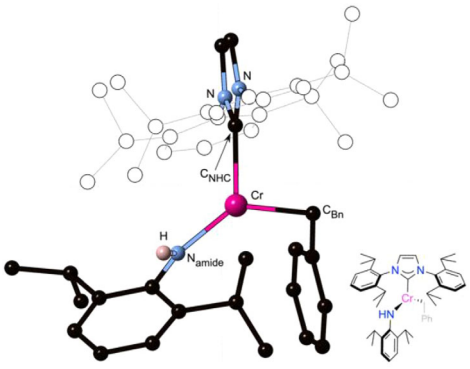

Figure 5. The structure of **6a** with selected metrical data (Å and °): Cr–C_{NHC} = 2.115(5); Cr–N_{amide} = 1.979(4); Cr–C_{Bn} = 2.105(6); C_{NHC}–Cr–C_{Bn} = 98.4(2); C_{NHC}–Cr–N_{amide} = 128.67(18); C_{Bn}–Cr–N_{amide} = 131.4(2), Cr–C_{Bn}–C_{ipso} = 104.3(4); Σ at Cr = 358.5.

operation of weak intramolecular, noncovalent cation-π interactions. In **2c** the geometry at Cr is considered as compressed-Y, planar approaching T-shaped (Σ = 360.0°), with longer Cr–C_{NHC} (2.135(11) Å) and distorted tetrahedral geometry at C_{Bn} (102–105°). It is pertinent to notice, though, that in **2c** an analysis of

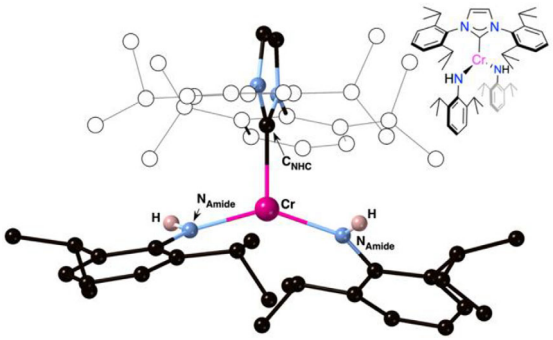

Figure 6. The structure of **7** with selected metrical data (Å and °): Cr–C_{NHC} = 2.081(3); Cr–N_{amide} = 1.983(2) and 1.974(2); N_{amide}–Cr–N_{amide} = 144.97(11); C_{NHC}–Cr–N_{amide} = 106.31(10) and 108.71(11); Σ at Cr = 359.9°.

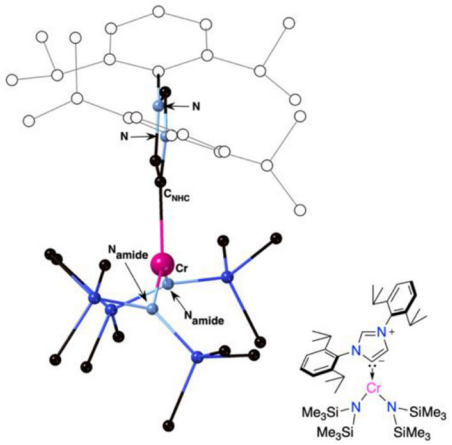

Figure 7. The structure of **8** with selected metrical data (Å and °): Cr–C_{NHC} = 2.1122(14); Cr–N_{amide} = 1.9937(12) and 2.0229(12); C_{NHC}–Cr–N_{amide} = 96.15(5) and 131.91(5); N_{amide}–Cr–N_{amide} = 131.47(5); Σ at Cr = 359.6°.

the geometrical distortions and their origin is hampered by (i) the presence of intermolecular close contacts which may influence the "open" three-coordinate geometry and (ii) the severe occupational disorder involving the Cr center and the Bn groups.

2.1.1. Structures and metrical data of the three-coordinate complexes 3, 4, 5a, 5b, 6a, 6b, 7 and 8

For the description of the geometries of the complexes **3**, **4**, **5a**, **5b**, **6a**, **6b**, **7** and **8** we chose two approaches which emphasize different structural aspects: (i) the classification by J. R. Gardinier et al.[47] for three-coordinate geometries, and (ii) the Continuous Shape Measures (CShM, generated by the SHAPE program[48]) as applied to three-coordinate geometries;[49] numerical data from the latter are provided in Table S2. By employing both approaches it is evident that pure trigonal planar (all coordination angles equal to 120°, idealized D_{3h} shape) geometries are only encountered in the complexes **3** and **4**. Near to ideal T-shaped geometries (one coordination angle equal to 180° and the other two equal to 90° (idealized C_{2v} shape) were not observed in any complex. However, all complexes are planar (sum of coordination angles Σ at Cr 359.6–360.1°, except **6b**,

which exhibits marginal pyramidalization (Σ = 352–356°). Planarity is also supported by the rather high CShMs from the two idealized C_{3v} shapes in the SHAPE outputs (Table S2). Based on the classification of J. R. Gardinier, complexes **5a**, **5b** and **6a** are best described as "compressed Y-shape", complex **8** as "extended Y-shape"; and complex **7** as approaching a T-shape geometry. Accordingly, the CShMs for **5a** and **5b** imply comparable distortions between trigonal planar (D_{3h}) and T-shaped (*mer*-trivacant octahedron C_{2v}) geometries (CShMs *ca*. 3 in both cases). Finally, complexes **6a**, **6b**, **7** and **8** are distorted trigonal planar rather than distorted T-shape (CShM *ca*. 1.4–1.8 and 3.6–8, respectively).

The fine structural variability may be attributed to the steric demands of the NHC and the amido coordination partners, the lowered rotation barriers around the Cr–C_{NHC} and Cr–N_{amido} bonds and the substantial number of energetically comparable conformations. In fact, torsional variablility is evidenced by the wide angle of torsional angles between the coordination and the NHC-heterocycle or the coordination and the N_{amido} planes (13–90° and 56–89°, respectively, see also Figures S22–S24 and Table S3). The need to maximize π-bonding between the Cr and the amido donors may also have an effect.

The Cr–C_{NHC} bond distances are slightly shorter in **7** and **8** possibly due to steric origins, but comparable in **3**, **4**, **5a**, **5b**, **6a** and **6b**, while the Cr–N_{amide} distances are the longest in **3**, **4** and **8**; both types of bond distances are falling in the range of the corresponding values reported in the literature.[31,46,50–52] Since **8** is the first Cr mesoionic, "abnormal" NHC complex, metrical data related to this bond for comparison type are nonexistent. In all complexes the minimum intermolecular close contacts and intermetallic distances are *ca*. 3.7 Å and 10.7 Å, respectively.

2.1.2. The scarcity of alkyl and abnormal NHC bis-silylamido complexes

The presence of both silylamido and σ-alkyl ligands on the same coordination sphere is uncommon: the neutral four-coordinate [M(R)($Ph_2PCH_2SiMe_2$)$_2$N], M = Cr, Co; R = Bn, CH_3,[53,54] and the "ato" three-coordinate [M(Bn){N($SiMe_3$)$_2$}$_2$)$^-K^+$], M = Fe,[55,56] Co,[56] Mn,[57] are rare examples of this type with 3*d* metals. Moreover, three-coordinate [M{N($SiMe_3$)$_2$}$_2$(*a*-ID*i*PP)] have been obtained for a limited number of bis-silylamides, either via one or two step metalation sequences (Zn,[58] Fe[55]) or by the thermal "normal-to-abnormal" rearrangement in toluene (Fe,[59] Co,[60]). Although the latter type of transformation is related to the conversion of **5b** to **8**, and its driving force should be attributed to the steric release and the increased bond energy of the M–*a*-ID*i*PP compared to M–ID*i*PP, the operating intimate mechanism of the rearrangement remains obscure. It is plausible to consider that it is either occurring in a concerted manner intermolecularly, by the involvement of bis-metalated ditopic NHCs, or after initial dissociation of the ID*i*PP, giving rise to transient [Cr{N($SiMe_3$)$_2$}$_2$], the latter at higher temperatures metalating at the "abnormal" position; the employment of a "protic" solvent,i.e. HN($SiMe_3$)$_2$, may facilitate proton mobility during the reaction.

2.1.3. The thermal stability of chromium bis-silylamido complexes

In order to obtain experimental evidence that high temperature "abnormal" intermolecular metalation by a [Cr{N($SiMe_3$)$_2$}$_2$] moiety may be feasible, complex **1**, considered as a plausible source of [Cr{N($SiMe_3$)$_2$}$_2$], was heated in the range 100–125°C in the presence or absence of ID*i*PP and in neat HN($SiMe_3$)$_2$ or *n*-octane as solvents. Although in the former case intractable Cr containing species and variable amounts of ID*i*PP were obtained, in the latter the tetranuclear complex **9** was isolated as brown crystalline material (Scheme 5 and Figure 8) after HN($SiMe_3$)$_2$ elimination and concomitant metalation of one CH_2-*H* of the N($SiMe_3$)$_2$ that remained on Cr. In the structure of **9**, there are two types of intermetallic distances within the Cr_4 square, 2.3598(13) and 2.4209(13) Å, comparable to the longer intermetallic distances in Cr_2^{4+} paddlewheel complexes;[61] nonsymmetric bridging, dianionic–{N($SiMe_3$)$_2$(μ^2–CH_2)} and (μ^2–N($SiMe_3$)$_2$ moieties hold also the Cr_4^{8+} core together. Related $SiMe_2$(CH_2-*H*) activations have been observed in other homoleptic (Ti,[62] V,[63]) and heteroleptic (Ti,[64,65] Zr,[65,66] Cr,[67] actinides[68]) silylamido species. A related tetranuclear complex with square arrangement of the metal atoms was reported in relation to the synthesis of [Cr{$CH_2Si(CH_3)_3$}$_4$] alkyls, where eight μ-CH_2SiMe_3 groups appear instead of the metalated silylamides of **9**;[69] a [(Ni^I{N($SiMe_3$)$_2$}$_4$] complex features also a square Ni_4^{4+} core and bridging N($SiMe_3$)$_2$ groups.[70] Finally, a linear tetranuclear Cr species has been obtained by dehydrogenation of one $SiMe_2$(CH_2–*H*) of the amido ligand –N(D*i*PP)$SiMe_3$ on attempted synthesis of chromium complexes.[71] In view of this thermal reactivity, the direct metalation of the ID*i*PP by [Cr{N($SiMe_3$)$_2$}$_2$] leading to **8** may be less likely.

2.2. Direct Current (DC) and Alternating Current (AC) Magnetic Measurements

The static and dynamic magnetic properties of complexes **3**, **5a**, **5b**, **6b** and **8** were investigated by DC magnetometry (see also Table 1). The temperature dependence of the product $\chi_M T(T)$ and the magnetic field dependence of the molar magnetization $M(H)$ for complexes **3**, **5a**, **5b**, **6b** and **8** are presented in Figures S28 and 9, respectively. At room temperature all investigated complexes show large deviations of the $\chi_M T$ from the spin-only value of 3.0 cm^3 K mol^{-1} expected for a high-spin $S = 2$ Cr^{II} complex. The $S = 2$ ground state would mean that the Cr^{II} in the investigated complexes is a non-Kramers magnetic ion. Simulations of $\chi_M T(T)$ and $M(H)$ dependencies using parameters (g_x, g_y, g_z, D, E) accurately determined experimentally by HFEPR (vide infra) do not match the DC magnetometry curves. However, the latter are compatible with a $S = 2$ system, the $\chi_M T$ value of which undergoes a marked decrease with decreasing temperature, indicating the presence of spin-orbit coupling. Attempts to include the orbital angular contribution in the fitting of the experimental data were unsuccessful, due to overparameterization. It should be stressed that, especially for systems in which there is significant orbital contribution,[16]

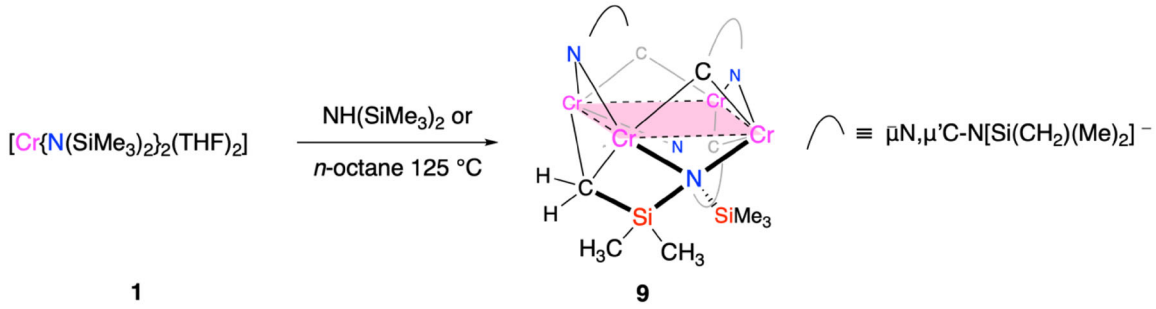

Scheme 5. Thermolysis of $[Cr\{N(SiMe_3)_2\}_2(THF)_2]$ (**1**) to the tetranuclear complex **9**.

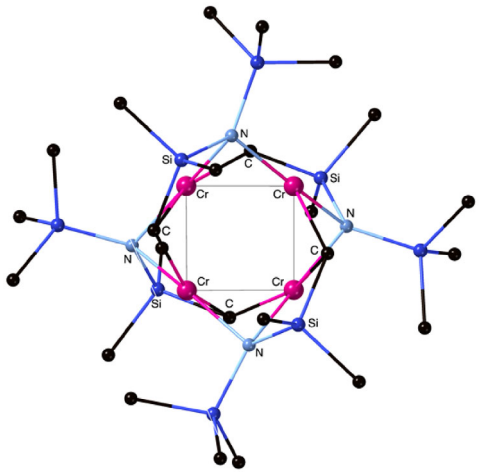

Figure 8. The structure of **9** with selected metrical data (Å): Cr–N = 2.070(5) and 2.124(5), Cr–C = 2.245(7) and 2.268(6), Cr–Cr = 2.3598(13) and 2.4209(13).

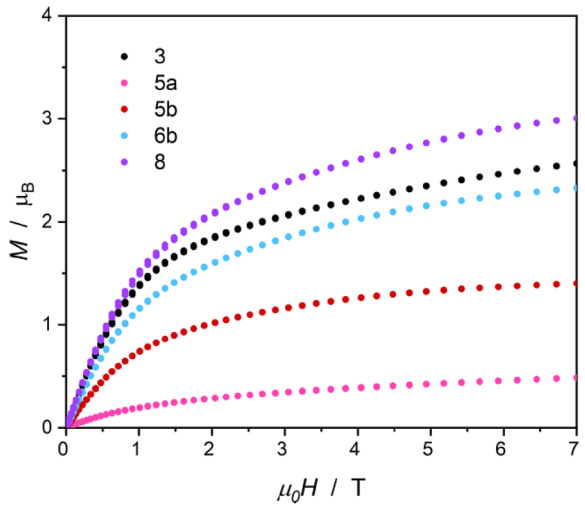

Figure 9. Magnetic field dependence of the molar magnetization for complexes **3**, **5a**, **5b**, **6b** and **8** at 1.8 K in the 0–7 T range.

a bulk technique like DC magnetometry alone cannot provide accurate *D* and *E* parameters.[72] To that end, HFEPR spectroscopy was employed as the most accurate method of choice[72] (vide infra).

The dynamic magnetic properties of complexes **3**, **5a**, **5b**, **6b** and **8** were studied by AC magnetometry in the 10–10 000 Hz frequency (ν) range. A generalized Debye model was used to fit AC magnetic susceptibility data (χ', $\chi''(\nu)$) and to extract the relaxation times τ (only for the complexes **5a**, **6b** and **8**). The field dependence of τ was measured at $T = 1.8$ K for each complex and was fit using the Equation 1:

$$\tau^{-1}(H) = A_1/\left(1 + A_2H^2\right) + A_3H^4 + A_4 \quad (1)$$

where, the first term describes quantum tunneling of magnetization (QTM) contribution, the second stands for the direct relaxation process, and the constant value A_4 is related to the contribution of the field-independent (Orbach and Raman) processes. Based on these results, the optimal DC magnetic field H_{DC}, *i.e.*, the field allowing to quench quantum tunneling of magnetization and therefore slow down the relaxation most effectively, was chosen for each complex. Then the temperature dependence of the χ', $\chi''(\nu)$ was studied at the optimal magnetic field H_{DC}. The values of the relaxation time τ extracted by the temperature dependence of the χ', $\chi''(\nu)$ were fit using Equation 2, including Raman (first term) and Orbach (second term) processes, if necessary:

$$\tau^{-1}(T) = CT^n + \tau_0^{-1}\exp\left(-U_{eff}/k_BT\right) \quad (2)$$

Complex **3** shows slow magnetization relaxation only after applying the optimal magnetic field $H_{DC} = 0.120$ T (Figure S29). Very short times of relaxation of magnetization do not allow to analyze the relaxation with the generalized Debye model (the $\chi''(\nu)$ maxima are above 10,000 Hz for $T > 1.9$ K (Figure S30)).

Complex **5a** also relaxes slowly under applied H_{DC} field (Figures S31 and S32). The temperature dependence of its magnetization relaxation was studied at 0.150 T up to $T = 2.6$ K (Figure S32). Moreover, the temperature dependence of τ^{-1} was fit only for Raman process (Equation 2) with parameters: $C = 1117(35)$ s^{-1} K^{-n}, $n = 4.32(4)$, $R^2 = 0.99861$ (Figure S33). The magnetization relaxation of complex **5b** is not slow enough to be analyzed (the maximum of χ'' falls above 10,000 Hz; Figure S35). The striking difference of the magnetization dynamics of the complexes **5a** and **5b** is remarkable and not fully understood, in view of their chemical and structural similarity (*cf.* Table S3). In fact, the structural differences between them originate from the unsaturation (**5a**) or saturation (**5b**) of the NHC backbone that is distant from the Cr center. This, in turn, affects conformations and torsional angles between the coordination, the amide, the

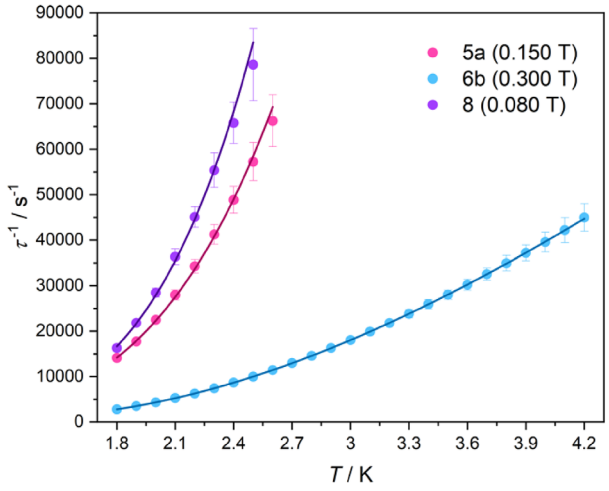

Figure 10. Comparison of the temperature dependence of τ^{-1} for complexes **5a** (H_{DC} = 0.150 T), **6b** (H_{DC} = 0.300 T) and **8** (H_{DC} = 0.080 T). The solid lines represent the best fits to Equation 2 for each case. Fitting parameters are the following: for **5a** (C = 1117(35) $s^{-1}K^{-n}$, n = 4.32(4), R^2 = 0.99861), for **6b** (C = 177(8) $s^{-1}K^{-n}$, n = 3.01(5), $\tau_0 = 2.74(6) \times 10^{-5}$ s, U_{eff} = 9.09(6) cm^{-1}, R^2 = 0.99999), and for **8** (C = 929(58) s^{-1} K^{-n}, n = 4.91(9), R^2 = 0.99627).

benzylic, and the NHC heterocycle planes (Figure S22), that may influence the magnetization relaxation.

The magnetization relaxation of complex **6b** is the slowest among the studied complexes (Figure 10), but it still needs nonzero static H_{DC} to quench QTM (Figure S36). Field dependence of τ was fit using Equation 1 with the following parameters: $A_1 = 4.7(7) \times 10^4$ s^{-1}, $A_2 = 7(1) \times 10^{-6}$ T^{-2}, $A_3 = 3(1) \times 10^{-13}$ $s^{-1}T^{-4}$, $A_4 = 2.1(1) \times 10^3$ s^{-1}, R^2 = 0.984 (Figure S37). The temperature dependence of τ was studied under an optimal magnetic field H_{DC} = 0.300 T up to 4.2 K (Figure S38) and fit using Equation 2 including both Raman and Orbach mechanisms: C = 177(8) s^{-1} K^{-n}, n = 3.01(5), $\tau_0 = 2.74(6) \times 10^{-5}$ s, U_{eff} = 9.09(6) cm^{-1}, R^2 = 1.00 (Figure S39). The magnitude of the U_{eff} is of a similar order of magnitude to those reported in the literature for mononuclear Cr^{II} field induced SIMs, Table S4.[32,33]

Similarly to other complexes studied here, complex **8** relaxes slowly only under an applied external H_{DC} magnetic field (Figure S40 and S41). The temperature dependence of relaxation time τ was studied at H_{DC} = 0.080 T up to T = 2.5 K (Figure S42). The temperature dependence of its τ^{-1} was fit with only Raman process (Equation 2) with parameters: C = 929(58) $s^{-1}K^{-n}$, n = 4.91(9), R^2 = 0.99627 (Figure S43). Figure 10 compares the temperature dependence of τ^{-1} for compounds **5a**, **6b** and **8**, showing that magnetic dynamics of complexes **5a** and **8** (only Raman relaxation mechanism) are very similar and faster than the ones for complex **6b** (Raman and Orbach mechanisms). It is worth noticing that a stronger applied H_{DC} field is required to block QTM for complex **6b** than for **5a** and **8**.

2.3. HFEPR Measurements

The complexes **3, 4, 5a, 5b** and **8** were subjected to HFEPR experiments to accurately determine the spin Hamiltonian (*sH*) parameters *D, E*, and *g*. Complexes **3**, **4,** and **8** feature two silylamido donors, while **5a** and **5b** have one silylamido and one benzyl donors in trigonal planar and "compressed Y" geometries, respectively (vide supra).

Complex **3** generated extraordinarily strong HFEPR response at any frequency at cryogenic temperatures. The resulting spectra could only be interpreted assuming an almost complete torquing (re-orientation) of the crystallites in the magnetic field,[73] with the *z*-axis of the zfs tensor parallel to the field (Figures S44 and S45 in the ESI). The resulting spectra are thus of a quasi-single-crystal quality. A comparison with simulations (colored traces in Figures S44 and S45) indicates that the sign of *D* is negative.

An attempt to prevent the complex from torquing by immersing it in *n*-eicosane mull was partly successful. The resulting HFEPR spectra shown in Figures S46 and S47 in the ESI lacked the characteristics of single-crystal ones but at the same time were not ideal powder patterns. The very small linewidth of individual crystallites resulted in the phenomenon of "quasi noise," also colloquially called "grass pattern" between the turning points, despite grinding the sample prior to immersing it in *n*-eicosane, observed previously for example in octahedral Mn(III) $3d^4$ systems.[74] The spectra recorded at the lower end of available frequencies (Figure S46) tended to be better than those at the high end (Figure S47). Despite the "quasi noise" problem, we were able to recognize enough turning points in the spectra to construct a 2D (field versus frequency) map of those points and perform the least-square fit of the *sH* parameters to this map according to the methodology of tunable-frequency EPR (Figure S48).[75] The parameters obtained in this way are shown in Table 2. A negative sign of *D* (–2.980 cm^{-1}) was confirmed.

Given the propensity of complex **3** to strongly torque in the magnetic field, complex **4** was measured only in *n*-eicosane mull. The resulting spectra are shown in Figure 11 (left panel) and S49 in the ESI, in each case accompanied by simulations using either positive or negative sign of *D*. These simulations confirmed that *D* is negative. The *sH* parameters of complex **4** were established from a 2D (field versus frequency) map of turning points (Figure 12, left panel) and are very similar to those of **3** which is consistent with the same description of the coordination geometry on the Cr^{II} ion (vide supra). These parameters can be found in Table 2.

Complex **5a** produced strong EPR response at any frequency at cryogenic temperatures. In stark contrast to complex **3**, it did not torque in magnetic field and the spectra could be adequately interpreted and simulated as powder patterns (Figure 11 middle panel). They allowed for a very precise determination of the *sH* parameters (Table 2) through the tunable frequency methodology quoted above (Figure 12, middle panel). The magnitude of *D* in **5a** is much smaller than in complexes **3** and **4,** 1.633 versus 2.980 and 2.927 cm^{-1}, while the rhombicity factor *E*/*D* is larger, 0.069 versus 0.026 and 0.036, respectively, though still very small. The sign of *D* is negative like in complexes **3** and **4,** as determined by simulations in Figure 11, middle panel. Two additional spectra and their simulations, at frequencies lower and higher, respectively, than that in Figure 11, are shown in Figures

Table 2. Spin Hamiltonian parameters determined by CASSCF + NEVPT2 calculations (normal font) and experimentally by HFEPR spectroscopy (bold font).

Complex	D	E/D	g_x	g_y	g_z
3	−2.99 **−2.980(3)**	0.024 **0.026**	1.917 **1.985(3)**	2.001 **1.993(2)**	2.001 **1.939(3)**
4	−2.90 **−2.927(4)**	0.027 **0.036**	1.920 **1.988(3)**	2.001 **1.988(3)**	2.001 **1.943(4)**
5a	−1.02 **−1.633(3)**	0.040 **0.069**	1.972 **1.998(2)**	2.002 **1.993(2)**	2.002 **1.984(3)**
5b	−0.98 **−1.663(3)**	0.038 **0.069**	1.974 **1.998(2)**	2.002 **1.993(2)**	2.002 **1.984(3)**
6b	−1.12	0.026	1.970	2.002	2.002
8	−1.85 **−2.305(3)**	0.020 **0.043**	1.947 **1.990(2)**	2.002 **1.995(2)**	2.002 **1.942(5)**

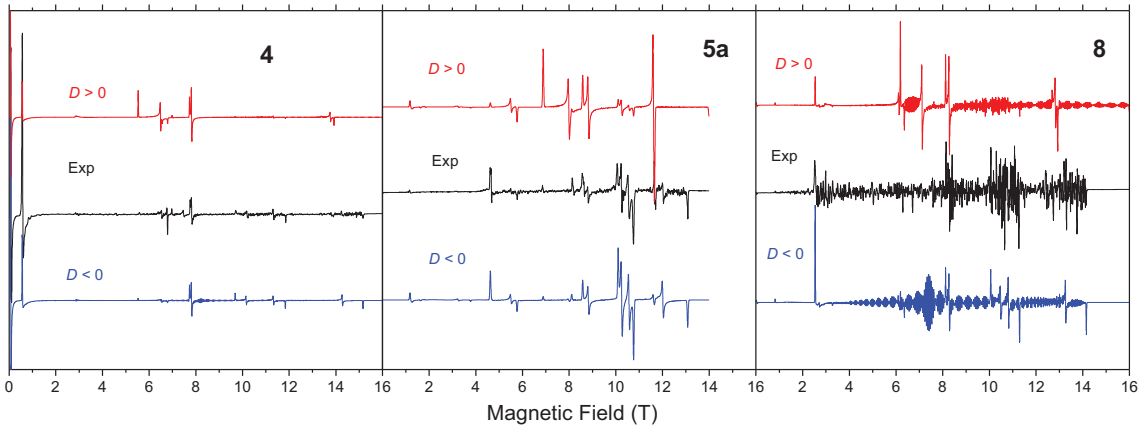

Figure 11. *Left*: The HFEPR spectrum of complex **4** in *n*-eicosane mull at 276 GHz and 10 K and its powder-pattern simulations using *sH* parameters as in Table 2. Black trace: experiment; red trace: simulation assuming positive D; blue trace: simulation assuming negative D. The frequency of 276 GHz corresponds to a value very close to the $|3D + 3E|$ zero-field energy gap, hence the presence of a resonance almost at zero field. *Middle*: The HFEPR spectrum of complex **5a** "as is" at 276 GHz and 10 K and its simulations assuming a powder distribution of the crystallites using *sH* parameters as in Table 2 except for $g_{iso} = 2.00$, with the same meaning of colors as before. *Right*: The HFEPR spectrum of complex **8** "as is" at 276 GHz and 10 K and its simulations assuming a powder distribution of the crystallites using *sH* parameters as in Table 2, with the same meaning of colors as before. Despite a strong "grass pattern" in the experimental spectrum that could not be overcome by grinding, enough turning points are recognizable to interpret the spectrum, particularly those at *ca.* 2.5 and 14 T. The simulations phenomenologically reproduce the "grass pattern" by assuming a small (10 mT) linewidth of individual crystallites.

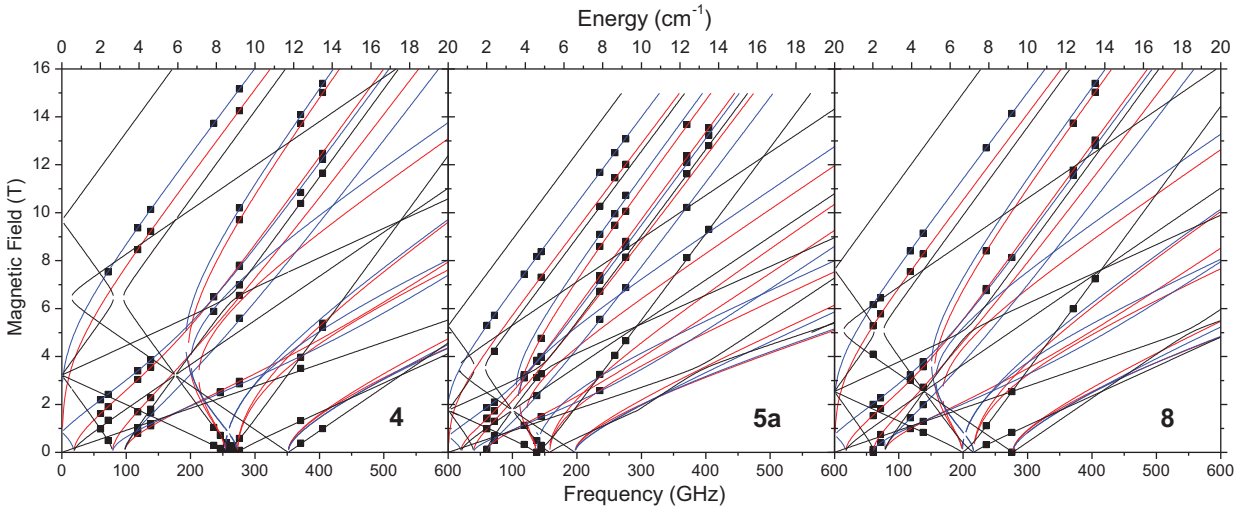

Figure 12. Maps of turning points in the EPR spectra at 10 K in complexes **4** (*left*), **5a** (*middle*) and **8** (*right*) as a function of frequency (energy). The squares are experimental points (canonical orientations only; off-axis turning points, of which there are many, are ignored). The lines are simulations using *sH* parameters[31] as in Table 2. Red lines: turning points with magnetic field parallel to the x zfs tensor axis; blue lines: $B_0 \parallel y$; black lines: $B_0 \parallel z$.

S50 and S51. The HFEPR spectra of **5b** (Figure S52) are almost identical to those of **5a**.

The final studied complex measured by HFEPR, **8**, showed a pronounced "grass pattern" both as loose powder, and in *n*-eicosane mull, even after being finely ground. Despite this phenomenon, the spectra, such as the ones shown in Figures 11 (right panel) and S53, showed enough identifiable turning points to get fully analyzed. The *sH* parameters (Table 2) were obtained from the fits to the 2D (field versus frequency) map of these points (Figure 12, right panel). The sign of *D* is negative like in all the series of complexes, and its magnitude (2.305 cm^{-1}) falls in between those of complexes **5a** and **5b** on the low side, and **3** and **4** on the high side.

2.4. Computational Studies

To probe the origin of the magnetic anisotropy in the isolated complexes, multireference ab initio SA-CASSCF/NEVPT2 calculations were performed based on the X-ray crystal and on DFT-optimized structures ignoring intermolecular effects (Tables S12 and S13). The quintet state was identified as the electronic ground state by optimizing the molecular geometries across all possible spin states, and this assignment was further validated using multireference methods. As there were only minor differences between the experimental and calculated ground state geometries, the subsequent results are derived from the crystal structures. It is noticed that all the investigated complexes possess a negative axial zfs parameter (*D*) with calculated values for complexes **3** and **5a** being -2.99 cm^{-1} and -1.02 cm^{-1}, respectively, (Table S14) consistent with HFEPR findings (Table 2). The magnitude of zfs directly correlates to the energy difference between the ground and the excited quintet states, with smaller energy differences leading to larger *D* values (Table S15).[76,77] The sign of *D* is determined by the excitation of an electron between two orbitals in a spin-conserved environment. This can occur in the same or opposite $|m_l|$ states, with a negative or positive contribution to *D*.[78,79] In this context, Nagelski et al. have investigated three-coordinate Fe^{II} and Co^{II} complexes using advanced spectroscopic techniques to accurately determine the zfs parameters, and effectively correlated the observed transition energies with computational data.[80] For complex **3,** the CASSCF-converged wavefunction elucidates that the major contribution to the ground-state configuration stems from the $d_{yz}^1\, d_{z^2}^1\, d_{xz}^1\, d_{x^2-y^2}^1\, d_{xy}^0$ configuration (Figure 13). The first excited state arises from the transition of an electron from $d_{x^2-y^2}$ to d_{xy} remaining within the same $|m_l|$ state, i.e., with $d_{yz}^1\, d_{z^2}^1\, d_{xz}^1\, d_{x^2-y^2}^0\, d_{xy}^1$ configuration. This results in a negative contribution to the *D* value. Moreover, the energy required for this transition is 4281 cm^{-1}, which leads to a smaller magnitude for the *D* parameter. For complex **5a**, $d_{yz}^1\, d_{z^2}^1\, d_{xz}^1\, d_{xy}^1\, d_{x^2-y^2}^0$ configuration comprises most of the ground state configuration (Figure 13). The first excited state adopts the $d_{yz}^1\, d_{z^2}^1\, d_{xz}^1\, d_{xy}^0\, d_{x^2-y^2}^1$ configuration, resulting from an electron transition from d_{xy} to $d_{x^2-y^2}$ requiring an energy of 11 288 cm^{-1}, and producing a small negative *D* value. The next higher energy transitions make a negligibly small contribution to the magnitude of *D*.

Due to the few relaxation pathways available, spin relaxation happens before the barrier is reached, i.e., under the effective energy barrier for complex **3**. Among the significant viable relaxation mechanistic pathways, QTM (quantum tunneling of magnetization) and TA-QTM (thermally assisted quantum tunneling of magnetization) serve as the through-barrier shortcuts between the $\pm M_S$ sublevels of the respective doubly degenerate states. For non-Kramers systems, QTM and TA-QTM are characterized by the tunnel splitting value ($\Delta_{tun.}$) between two degenerate $\pm M_S$ sublevels.[77] For complex **3**, the minimal tunnel splitting value ($\Delta_{tun.} = 0.006$) in the ground state rules out the possibility of quantum tunneling of magnetization in the ground state. As a result, this complex will exhibit magnetization relaxation through thermally assisted quantum tunneling in the first excited state, as illustrated by the qualitative blocking barrier plot (Figure S54). In such case, the energy gap between the ground state and the first excited state dictates the effective barrier to magnetization reversal (U_{eff}). So, complex **3** is observed with U_{eff} value of 8.97 cm^{-1} (Figure S54). Similarly, for complex **5a**, the tunneling splitting value in the ground ($M_S = \pm 2$) levels is very small (0.005 cm^{-1}), while it is significant in the excited $M_S = \pm 1$ levels (Figure S54). Thus, this complex will undergo magnetization relaxation through quantum tunneling involving the first excited state, yielding an U_{eff} value of 3.08 cm^{-1}. While all the complexes display negative *D* values, complexes **3**, **4**, and **8** among the studied systems show a relatively larger magnitude of *D*, ranging from ≈ -1.8 to -3.0 cm^{-1}. The axial zfs parameters for the remaining complexes have been estimated, and Table 2 presents the corresponding calculated *D*, *E*/*D*, and *g*-values.

3. Conclusions

In conclusion, we have reported the synthesis of a family of novel three-coordinate paramagnetic ($S = 2$) bis-amido- and amido-benzyl-NHC complexes of Cr^{II} by substitution or aminolysis and thermolysis methods from $[Cr\{N(SiMe_3)_2\}_2(THF)_2]$ or $[Cr(IDippPP)Bn_2]$ and $[Cr(SIDippPP)Bn_2]$, respectively. The complexes display fine structural variation among the trigonal planar, extended-Y, compressed-Y, and T-shape extremes. For these complexes, DC magnetometry data cannot furnish accurate *sH* parameters, due to overparameterization. This difficulty was overcome by employing HFEPR spectroscopy to obtain benchmark values for five representative complexes (**3**, **4**, **5a**, **5b**, **8**). The high quality of the obtained spectra enabled the complete and accurate determination of their *sH* parameters. Moreover, the corresponding *D* and *E*/*D* computed values are in excellent, for **3** and **4**, and in reasonable agreement for the rest of the complexes. Both HFEPR-derived and computed *D* values are negative ranging between $-1.663(3)$ and $-2.980(3)$ cm^{-1}. Interestingly, the trigonal planar **3** and **4** exhibited the largest $|D|$ values and the lowest rhombicities (*E*/*D*), while the most deviating from the trigonal planar shapes **5a** and **5b** displayed the smallest $|D|$ and the largest rhombicities; the $|D|$ and *E*/*D* values of complex

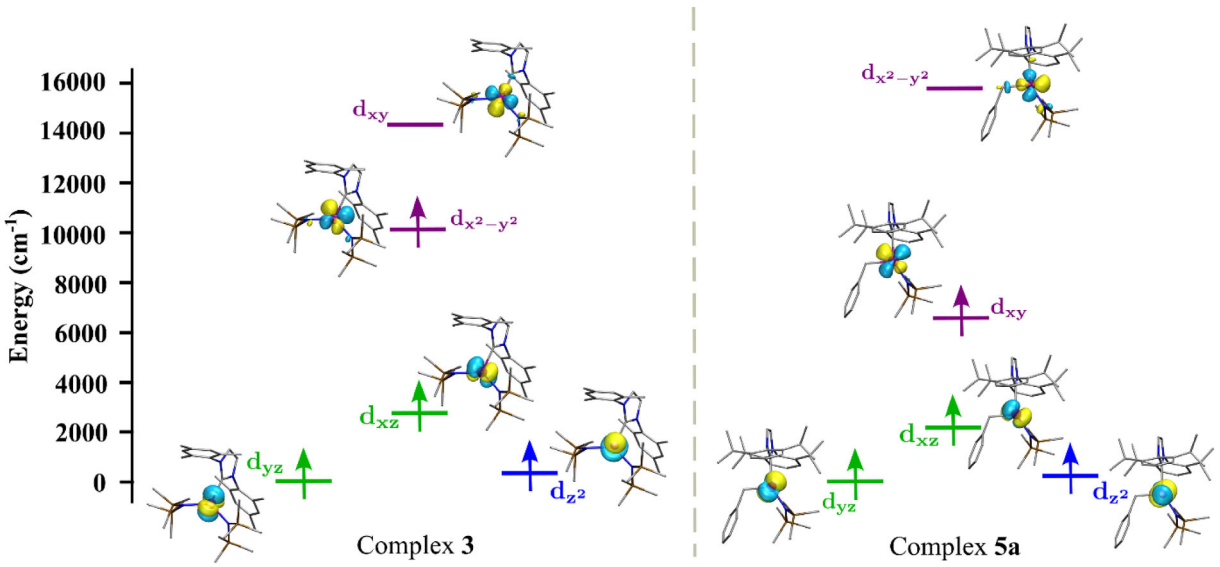

Figure 13. The *d*-orbital splitting pattern in the ground state computed using CAS(4,5)+NEVPT2 for complex **3** (left) and **5a** (right), with the molecular orbitals (MOs) plotted at an *iso*-value of 0.05 μ_B. Color coding: green for d_{xz} and d_{yz} MO energy levels with its respective electrons (arrows), blue for d_z^2 and violet for d_{xy} and $d_{x^2-y^2}$.

8 fell between the previous extremes (Table 2). Noticeably, the *D* values of Cr^{II} complexes found in the literature span a range between –1.71(11) and –2.01(1) cm^{-1}, and *E*/*D* between 0.0054 and 0.049, while complex V (in Table S4) shows DC magnetometry-derived $D = \pm 1.92(3)$ cm^{-1} and $E/D = 0.29(2)$. The negative *D*, combined with the moderate rhombicities of the complexes presented herein, would, in principle, lead to slow magnetization relaxation.[10] AC magnetometry supported this surmise for **5a**, **6b** and **8** only, that adhere either to Raman (**5a** and **8**) or combined Raman/Orbach (**6b**) field-induced relaxation mechanisms. It should be noted that computational results for complexes **3** and **5a** (which did not take into account intermolecular interactions) were analyzed according to the Orbach relaxation mechanism (vide infra). Overall, the present combined experimental and computational work expands the existing magnetostructural correlations for high-spin Cr^{II} complexes by the introduction of three-coordinate geometries. It would be of interest to further elucidate the dynamic magnetic behavior of these and related species by exploring possibly operating spin-phonon interactions, which are currently under detailed scrutiny for both 3*d* metal- and lanthanide -based SIMs.[16,81–84]

Supporting Information

The Supporting Information for this manuscript contains full details of synthetic procedures for new compounds, characterization data, representative paramagnetic ^{1}H-NMR spectra, HFEPR spectra, details of magnetic measurements, details of computational calculations and full crystallographic details for all the structurally characterized complexes, including data of the cyclometalated component **3a** (cocrystallized with **3**) and the binuclear precursor to **2c** (Scheme 2) featuring a distorted four-coordinate geometry at Cr ($\tau'_4 = 0.29$); comparative views of the related **5a**, **5b** (sharing the $N(SiMe_3)_2$ and Bn ligation but differing in the ID*i*PP and sID*i*PP ligands), **6a**, **6b** (sharing the NHD*i*PP and Bn ligation but differing in the ID*i*PP and sID*i*PP ligands), and **3**, **4** and **8** (sharing the two $N(SiMe_3)_2$ ligation but differing in the IMes, ID*i*PP and *a*ID*i*PP). CIFs are available from https://www.ccdc.cam.ac.uk/structures/. CCDC Numbers are: 2423359, 2242263, 2420539, 2420806, 2421413, 2421414, 2421417, 2421418, 2421429, 2421431, 2421432, 2422263, 2242264. The authors have cited additional references within the Supporting Information.

Acknowledgments

This work was partly financed by the National Science Centre Poland within the Opus project 2020/37/B/ST5/02735. The authors acknowledge the DUS grant from the Faculty of Chemistry under the Strategic Programme Excellence Initiative at the Jagiellonian University. The study was partly carried out using the research infrastructure cofounded by the European Union in the framework of the Smart Growth Operational Program, Measure 4.2; Grant No. POIR.04.02.00–00-D001/20, "ATOMIN 2.0–ATOMic scale science for the INnovative economy". We also acknowledge the Special Account for Research Grants of the National and Kapodistrian University of Athens (A.A.D and P.K.), the CNRS and the University of Strasbourg (A.A.D and P.B.) and the Department of Science and Technology (India) through SERB-CRG project no. CRG/2019/003237 (M.E.A) for financial support. The single crystal diffraction data of the complexes **2b**, **2c**, **3**, **5b**, **6b** and **8** were collected in the National and Kapodistrian University of Athens X-Ray Diffraction Facility. Part of this work was performed at the National High Magnetic Field Laboratory which is supported by NSF Cooperative Agreement No. DMR-2128556 and the State of Florida. We thank Dr. A. Ozarowski for his simulation

and fitting program SPIN, and one anonymous reviewer for many constructive comments.

Conflict of Interest

The authors declare no conflict of interest.

Data Availability Statement

The data that support the findings of this study are available in the supplementary material of this article.

Keywords: carbene ligands · chromium · computational chemistry · EPR spectroscopy · Magnetic properties

[1] C. J. Milios, R. E. P. Winpenny, in *Molecular Nanomagnets and Related Phenomena*, Structure and Bonding, Vol. *164*, (Ed.: S. Gao), **2015**, pp. 1–109.
[2] N. Ishikawa, M. Sugita, T. Ishikawa, S.-y. Koshihara, Y. Kaizu, *J. Am. Chem. Soc.* **2003**, *125*, 8694.
[3] F.-S. Guo, B. M. Day, Y.-C. Chen, M.-L. Tong, A. Mansikkamäki, R. A. Layfield, *Angew. Chem., Int. Ed.* **2017**, *56*, 11445.
[4] F.-S. Guo, B. M. Day, Y.-C. Chen, M.-L. Tong, A. Mansikkamäki, R. A. Layfield, *Science* **2018**, *362*, 1400.
[5] C. A. P. Goodwin, F. Ortu, D. Reta, N. F. Chilton, D. P. Mills, *Nature* **2017**, *548*, 439.
[6] C. A. Gould, K. R. McClain, D. Reta, J. G. C. Kragskow, D. A. Marchiori, E. Lachman, E.-S. Choi, J. G. Analytis, R. D. Britt, N. F. Chilton, B. G. Harvey, J. R. Long, *Science* **2022**, *375*, 198.
[7] A. Zabala-Lekuona, J. M. Seco, E. Colacio, *Coord. Chem. Rev.* **2021**, *441*, 213984.
[8] D. E. Freedman, W. H. Harman, T. D. Harris, G. J. Long, C. J. Chang, J. R. Long, *J. Am. Chem. Soc.* **2010**, *132*, 1224.
[9] G. A. Craig, M. Murrie, *Chem. Soc. Rev.* **2015**, *44*, 2135.
[10] J. M. Frost, K. L. M. Harriman, M. Murugesu, *Chem. Sci.* **2016**, *7*, 2470.
[11] M. Feng, M.-L. Tong, *Chem. Eur. J.* **2018**, *24*, 7574.
[12] J. M. Zadrozny, D. J. Xiao, M. Atanasov, G. J. Long, F. Grandjean, F. Neese, J. R. Long, *Nat. Chem.* **2013**, *5*, 577.
[13] A. A. Danopoulos, P. Braunstein, K. Y. Monakhov, J. van Leusen, P. Kögerler, M. Clémancey, J.-M. Latour, A. Benayad, M. Tromp, E. Rezabal, G. Frison, *Dalton Trans.* **2017**, *46*, 1163.
[14] R. Weller, M. Atanasov, S. Demeshko, T.-Y. Chen, I. Mohelsky, E. Bill, M. Orlita, F. Meyer, F. Neese, C. G. Werncke, *Inorg. Chem.* **2023**, *62*, 3153.
[15] A. J. Valentine, A. M. Geer, T. J. Blundell, W. Tovey, M. J. Cliffe, E. S. Davies, S. P. Argent, W. Lewis, J. McMaster, L. J. Taylor, D. Reta, D. L. Kays, *Dalton Trans.* **2022**, *51*, 18118.
[16] J. M. Zadrozny, M. Atanasov, A. M. Bryan, C.-Y. Lin, B. D. Rekken, P. P. Power, F. Neese, J. R. Long, *Chem. Sci.* **2013**, *4*, 125.
[17] Y.-S. Meng, Z. Mo, B.-W. Wang, Y.-Q. Zhang, L. Deng, S. Gao, *Chem. Sci.* **2015**, *6*, 7156.
[18] X.-N. Yao, J.-Z. Du, Y.-Q. Zhang, X.-B. Leng, M.-W. Yang, S.-D. Jiang, Z.-X. Wang, Z.-W. Ouyang, L. Deng, B.-W. Wang, S. Gao, *J. Am. Chem. Soc.* **2017**, *139*, 373.
[19] R. C. Poulten, M. J. Page, A. G. Algarra, J. J. Le Roy, I. López, E. Carter, A. Llobet, S. A. Macgregor, M. F. Mahon, D. M. Murphy, M. Murugesu, M. K. Whittlesey, *J. Am. Chem. Soc.* **2013**, *135*, 13640.
[20] Y.-F. Deng, Z. Wang, Z.-W. Ouyang, B. Yin, Z. Zheng, Y.-Z. Zheng, *Chem. Eur. J.* **2016**, *22*, 14821.
[21] C. G. Werncke, L. Vendier, S. Sabo-Etienne, J.-P. Sutter, C. Pichon, S. Bontemps, *Eur. J. Inorg. Chem.* **2017**, *2017*, 1041.
[22] M. R. Saber, J. A. Przyojski, Z. J. Tonzetich, K. R. Dunbar, *Dalton Trans.* **2020**, *49*, 11577.
[23] C. Das, A. Rasamsetty, S. Tripathi, M. Shanmugam, *Chem. Commun.* **2020**, *56*, 13397.
[24] J. Jung, C. M. Legendre, S. Demeshko, R. Herbst-Irmer, D. Stalke, *Inorg. Chem.* **2021**, *60*, 9580.
[25] S. Indris, T. Bredow, B. Schwarz, A. Eichhöfer, *Inorg. Chem.* **2022**, *61*, 554.
[26] P.-H. Lin, N. C. Smythe, S. I. Gorelsky, S. Maguire, N. J. Henson, I. Korobkov, B. L. Scott, J. C. Gordon, R. T. Baker, M. Murugesu, *J. Am. Chem. Soc.* **2011**, *133*, 15806.
[27] Y. Li, J. Xi, J. Ferrando-Soria, Y.-Q. Zhang, W. Wang, Y. Song, Y. Guo, E. Pardo, X. Liu, *Dalton Trans.* **2022**, *51*, 8266.
[28] N. Ge, Y.-Q. Zhai, Y.-F. Deng, Y.-S. Ding, T. Wu, Z.-X. Wang, Z. Ouyang, H. Nojiri, Y.-Z. Zheng, *Inorg. Chem. Front.* **2018**, *5*, 2486.
[29] S. Indris, M. Knapp, B. Schwarz, A. Eichhöfer, *Eur. J. Inorg. Chem.* **2021**, *2021*, 951.
[30] D. C. Bradley, M. B. Hursthouse, C. W. Newing, A. J. Welch, *J. Chem. Soc., Chem. Commun.* **1972**, 567.
[31] Y.-F. Deng, T. Han, Z. Wang, Z. Ouyang, B. Yin, Z. Zheng, J. Krzystek, Y.-Z. Zheng, *Chem. Commun.* **2015**, *51*, 17688.
[32] J. Su, L. Yin, Z. Ouyang, Z. Wang, W. Zheng, *Dalton Trans.* **2020**, *49*, 6945.
[33] Y.-Q. Zhai, N. Ge, Z.-H. Li, W.-P. Chen, T. Han, Z.-W. Ouyang, Z. Wang, Y.-Z. Zheng, *Inorg. Chem.* **2021**, *60*, 1344.
[34] Q.-C. Luo, N. Ge, Y.-Q. Zhai, T.-B. Wang, L. Sun, Q. Sun, F. Li, Z. Ouyang, Z.-X. Wang, Y.-Z. Zheng, *Dalton Trans.* **2022**, *51*, 9218.
[35] I. C. Cai, M. I. Lipschutz, T. D. Tilley, *Chem. Commun.* **2014**, *50*, 13062.
[36] K. Freitag, C. R. Stennett, A. Mansikkamäki, R. A. Fischer, P. P. Power, *Inorg. Chem.* **2021**, *60*, 4108.
[37] H. Chen, R. A. Bartlett, M. M. Olmstead, P. P. Power, S. C. Shoner, *J. Am. Chem. Soc.* **1990**, *112*, 1048.
[38] J. N. Boynton, W. A. Merrill, W. M. Reiff, J. C. Fettinger, P. P. Power, *Inorg. Chem.* **2012**, *51*, 3212.
[39] K.-C. Hsiao, P.-C. Yang, C.-T. Fang, H.-K. Liu, C.-Y. Lin, *Chem. Asian J.* **2024**, *19*, e202300924.
[40] S. N. König, C. Schädle, C. Maichle-Mössmer, R. Anwander, *Inorg. Chem.* **2014**, *53*, 4585.
[41] A. Sarkar, R. Jose, H. Ghosh, G. Rajaraman, *Inorg. Chem.* **2021**, *60*, 9680.
[42] S. Gopal Patra, P. Kumar Chattaraj, *Polyhedron* **2024**, *256*, 116990.
[43] Y. Li, Z. Zeng, Y. Guo, X. Liu, Y.-Q. Zhang, Z. Ouyang, Z. Wang, X. Liu, Y.-Z. Zheng, *Inorg. Chem.* **2023**, *62*, 6297.
[44] R. A. Layfield, J. J. W. McDouall, M. Scheer, C. Schwarzmaier, F. Tuna, *Chem. Commun.* **2011**, *47*, 10623.
[45] A. Massard, P. Braunstein, A. A. Danopoulos, S. Choua, P. Rabu, *Organometallics* **2015**, *34*, 2429.
[46] A. A. Danopoulos, K. Y. Monakhov, V. Robert, P. Braunstein, R. Pattacini, S. Conde-Guadaño, M. Hanton, R. P. Tooze, *Organometallics* **2013**, *32*, 1842.
[47] T. L. Davis, J. L. Watts, K. J. Brown, J. S. Hewage, A. R. Treleven, S. V. Lindeman, J. R. Gardinier, *Dalton Trans.* **2015**, *44*, 15408.
[48] *SHAPE*, M. Llunell, D. Casanova, J. Cirera, P. Alemany, S. Alvarez, Universitat de Barcelona, Barcelona **2013**.
[49] S. Alvarez, *Eur. J. Inorg. Chem.* **2021**, *2021*, 3632.
[50] S. Conde-Guadano, A. A. Danopoulos, R. Pattacini, M. Hanton, R. P. Tooze, *Organometallics* **2012**, *31*, 1643.
[51] J. Wang, G. Tan, D. An, H. Zhu, Y. Yang, *Z. Anorg. Allg. Chem.* **2011**, *637*, 1597.
[52] G. Horrer, M. S. Luff, U. Radius, *Dalton Trans.* **2023**, *52*, 13244.
[53] M. D. Fryzuk, D. B. Leznoff, S. J. Rettig, *Organometallics* **1995**, *14*, 5193.
[54] M. D. Fryzuk, D. B. Leznoff, R. C. Thompson, S. J. Rettig, *J. Am. Chem. Soc.* **1998**, *120*, 10126.
[55] L. C. H. Maddock, T. Cadenbach, A. R. Kennedy, I. Borilovic, G. Aromí, E. Hevia, *Inorg. Chem.* **2015**, *54*, 9201.
[56] C. G. Werncke, J. Pfeiffer, I. Müller, L. Vendier, S. Sabo-Etienne, S. Bontemps, *Dalton Trans.* **2019**, *48*, 1757.
[57] R. Weller, L. Völlinger, C. G. Werncke, *Eur. J. Inorg. Chem.* **2021**, *2021*, 4383.
[58] J. B. Waters, J. M. Goicoechea, *Dalton Trans.* **2014**, *43*, 14239.
[59] B. M. Day, T. Pugh, D. Hendriks, C. F. Guerra, D. J. Evans, F. M. Bickelhaupt, R. A. Layfield, *J. Am. Chem. Soc.* **2013**, *135*, 13338.
[60] B. M. Day, K. Pal, T. Pugh, J. Tuck, R. A. Layfield, *Inorg. Chem.* **2014**, *53*, 10578.
[61] F. A. Cotton, in *Multiple Bonds Between Metal Atoms* (Eds.: F. A. Cotton, C. A. Murillo, R. A. Walton), Springer Science and Business Media Inc., New York **2005**, pp. 35–68.
[62] M. A. Putzer, J. Magull, H. Goesmann, B. Neumüller, K. Dehnicke, *Chem. Ber.* **1996**, *129*, 1401.

[63] P. Berno, S. Gambarotta, *Organometallics* **1994**, *13*, 2569.
[64] C. R. Bennett, D. C. Bradley, *J. Chem. Soc., Chem. Commun.* **1974**, 29.
[65] S. J. Simpson, R. A. Andersen, *Inorg. Chem.* **1981**, *20*, 3627.
[66] R. P. Planalp, R. A. Andersen, A. Zalkin, *Organometallics* **1983**, *2*, 16.
[67] R. Messere, M.-R. Spirlet, D. Jan, A. Demonceau, A. F. Noels, *Eur. J. Inorg. Chem.* **2000**, *2000*, 1151.
[68] S. J. Simpson, H. W. Turner, R. A. Andersen, *Inorg. Chem.* **1981**, *20*, 2991.
[69] C. Schulzke, D. Enright, H. Sugiyama, G. LeBlanc, S. Gambarotta, G. P. A. Yap, L. K. Thompson, D. R. Wilson, R. Duchateau, *Organometallics* **2002**, *21*, 3810.
[70] M. Faust, A. M. Bryan, A. Mansikkamäki, P. Vasko, M. M. Olmstead, H. M. Tuononen, F. Grandjean, G. J. Long, P. P. Power, *Angew. Chem., Int. Ed.* **2015**, *54*, 12914.
[71] C.-Y. Lin, J.-D. Guo, J. C. Fettinger, S. Nagase, F. Grandjean, G. J. Long, N. F. Chilton, P. P. Power, *Inorg. Chem.* **2013**, *52*, 13584.
[72] J. Krzystek, J. Telser, *Dalton Trans.* **2016**, *45*, 16751.
[73] T. Dubroca, A. Ozarowski, Y. Sunatsuki, J. Telser, S. Hill, J. Krzystek, *Appl. Magn. Reson.* **2025**, *56*, 137.
[74] A. P. Forshaw, J. M. Smith, A. Ozarowski, J. Krzystek, D. Smirnov, S. A. Zvyagin, T. D. Harris, H. I. Karunadasa, J. M. Zadrozny, A. Schnegg, K. Holldack, T. A. Jackson, A. Alamiri, D. M. Barnes, J. Telser, *Inorg. Chem.* **2013**, *52*, 144.
[75] J. Krzystek, S. A. Zvyagin, A. Ozarowski, S. Trofimenko, J. Telser, *J. Magn. Reson.* **2006**, *178*, 174.
[76] R. Maurice, R. Bastardis, C. d. Graaf, N. Suaud, T. Mallah, N. Guihéry, *J. Chem. Theory Comput.* **2009**, *5*, 2977.
[77] R. Khurana, S. Gupta, M. E. Ali, *J. Phys. Chem. A* **2021**, *125*, 2197.
[78] B. Cahier, R. Maurice, H. Bolvin, T. Mallah, N. Guihéry, *Magnetochemistry* **2016**, *2*, 31.
[79] S. Nain, A. Mukhopadhyaya, M. E. Ali, *Inorg. Chem.* **2024**, *63*, 7401.
[80] A. L. Nagelski, M. Ozerov, M. S. Fataftah, J. Krzystek, S. M. Greer, P. L. Holland, J. Telser, *Inorg. Chem.* **2024**, *63*, 4511.
[81] J. G. C. Kragskow, A. Mattioni, J. K. Staab, D. Reta, J. M. Skelton, N. F. Chilton, *Chem. Soc. Rev.* **2023**, *52*, 4567.
[82] S. Nain, M. Kumar, M. E. Ali, *Phys. Chem. Chem. Phys.* **2023**, *25*, 14848.
[83] K. Kotrle, M. Atanasov, F. Neese, R. Herchel, *Inorg. Chem.* **2023**, *62*, 17499.
[84] A. Mattioni, J. K. Staab, W. J. A. Blackmore, D. Reta, J. Iles-Smith, A. Nazir, N. F. Chilton, *Nat. Commun.* **2024**, *15*, 485.

Manuscript received: March 26, 2025
Revised manuscript received: June 12, 2025
Version of record online: ■■, ■■

RESEARCH ARTICLE

Some members of a family of three-coordinate $S = 2$ Cr^{II} complexes bearing NHC and amido donors display field-induced slow magnetization relaxation. Magnetostructural correlations are drawn within this family, and comparisons are made with literature Cr^{II} SIMs.

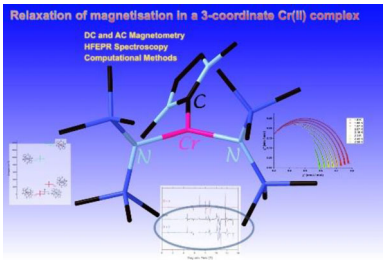

G. Handzlik, I. Ligielli, S. Nain, R. Khurana, M. E. Ali, E. Papangelis, C. Papapanagis, C. Bailly, N. Tsoureas, M. Danopoulou, C. Bethanis, P. Braunstein, D. Pinkowicz, J. Krzystek, P. Kyritsis, A. A. Danopoulos

1 – 13

Relaxing amid Three: Slow Magnetization Relaxation in Three-Coordinate Chromium(II) N-Heterocyclic Carbene Complexes